

Characterization of the in vivo wall shear stress environment of human fetus umbilical arteries and veins

Shier Nee Saw¹ · Chia Dawn² · Arijit Biswas² · Citra Nurfarah Zaini Mattar² · Choon Hwai Yap¹ 

Received: 9 May 2016 / Accepted: 20 July 2016 / Published online: 25 July 2016
© Springer-Verlag Berlin Heidelberg 2016

Abstract The endothelial cells of the umbilical vessels are frequently used in mechanobiology experiments. They are known to respond to wall shear stress (WSS) of blood flow, which influences vascular growth and remodeling. The in vivo environment of umbilical vascular WSS, however, is not well characterized. In this study, we performed detailed characterization of the umbilical vascular WSS environments using clinical ultrasound scans combined with computational simulations. Doppler ultrasound scans of 28 normal human fetuses from 32nd to 33rd gestational weeks were investigated. Vascular cross-sectional areas were quantified through 3D reconstruction of the vascular geometry from 3D B-mode ultrasound images, and flow velocities were quantified through pulse wave Doppler. WSS in umbilical vein was computed with Poiseuille's equation, whereas WSS in umbilical artery was obtained via computational fluid dynamics simulations of the helical arterial geometry. Results showed that blood flow velocity for umbilical artery and vein did not correlate with vascular sizes, suggesting that velocity had a very weak trend with or remained constant over vascular sizes. Average WSS for umbilical arteries and vein was 2.81 and 0.52 Pa, respectively. Umbilical vein WSS showed a significant negative correlation with the vessel diameter, but umbilical artery did not show any correlation. We hypothesize that this may be due to differential regulation of vascular sizes based on WSS sensing. Due to the helical geometry of

umbilical arteries, bending of the umbilical cord did not significantly alter the vascular resistance or WSS, unlike that in the umbilical veins. We hypothesize that the helical shape of umbilical arteries may be an adaptation feature to render a higher constancy of WSS and flow in the arteries despite umbilical cord bending.

Keywords Wall shear stress · Umbilical vein · Helical umbilical artery · Computational fluid dynamics

1 Introduction

It is well known that there is a remarkable correlation between blood flow and vessel diameter (Smiesko et al. 1985) whereby alteration of blood flow will affect the shear stress exerted on the endothelial cells (ECs), which signals for the growth and remodeling of the vessel and, hence, regulates the vessel's diameter. The regulation of vessel's diameter is dependent on the cell proliferation and migration of ECs that are lining on the interior surface of blood vessels (Nakatsu et al. 2003). Blood flow wall shear stress (WSS) is known to regulate factors such as VEGF, eNOS, and PDGF (Cheng et al. 2005; dela Paz et al. 2012; Hsieh et al. 1991), which in turn control the tone and growth of the vessel. Nakatsu et al. (2003) showed that different concentrations of VEGF will affect the various aspects of vascular growth, in terms of sprouting, elongation, branching and lumen formation. Others have shown that eNOS and PDGF are to be involved in regulating the vascular tone and are affected by the WSS in blood vessels (Cheng et al. 2005; Hsieh et al. 1991).

In the fetal circulation, phenomenological observations have corroborated with the above studies on the biochemical role of WSS in vascular growth and remodeling. For example, Struijk et al. (2005) showed that WSS in fetal aorta remained

✉ Choon Hwai Yap
bieyapc@nus.edu.sg

¹ Department of Biomedical Engineering, National University of Singapore, 9 Engineering Drive 1, #02-04, Singapore 117575, Singapore

² Department of Obstetrics and Gynecology, Yong Loo Lin School of Medicine, National University of Singapore, National University Health Systems, Singapore, Singapore

constant as the gestational age increased, and suggested that the fetal aorta adapts to flow demands to maintain constant mean WSS, via WSS regulation of vascular growth. Yap et al. (2014) reported similar observations in fetal mouse aortas and suggested that the fetal vasculature remodeled its size to maintain a WSS homeostasis. Collectively, these studies demonstrated the importance of understanding the WSS and fluid mechanical environment of the fetal circulation.

The quantification of WSS is especially important in umbilical vessels because ECs of umbilical artery and vein are popular sources of cells for the study of the biological response of ECs under varying WSS conditions (Traub and Berk 1998; Yoshizumi et al. 1989). Despite these numerous studies, the *in vivo* WSS environment of the umbilical artery and veins has not been formally investigated based on the clinical measurements of sufficient sample sizes. Recent studies using umbilical ECs have mostly adopted 4–25 dynes/cm² as a simulation of adult WSS environment (Malek et al. 1999; Nagel et al. 1999). However, it is important to understand the WSS environment of these cell sources in their native environment, which may have implications of their subsequent behaviors under *in vitro* experiments.

Studying the relationship between vascular sizes and WSS of the umbilical vessels also has relevance to the intrauterine growth restriction (IUGR) disease, whereby the placenta pathologically restricts fetal blood flow into fetus, resulting in insufficient transfer of nutrients and oxygen to the fetus. Fetus affected by IUGR (about 3% of all births) will suffer from growth restriction and consequently much high rates of mortality and long-term morbidity compared to normal fetus (Gardosi et al. 2009; Lawn et al. 2005). In IUGR, both the umbilical arteries and veins experience a reduction in flow velocities (Boito et al. 2002; Vinkesteijn et al. 2004) and vascular sizes (Boito et al. 2002; Raio et al. 2003), suggesting that the flow resistance in the umbilical vessels has increased. Since significant pressure losses can occur across the umbilical vessels (Kaplan et al. 2010), umbilical vascular resistance may exacerbate the high resistance of umbilical-placental circulation. It would be important to study vascular blood flow mechanics, to understand what controls the growth and remodeling of these vessels, so as to derive strategies to reduce vascular resistance and alleviate IUGR. In the current study, we strive to understand the WSS environment in healthy pregnancies as the first step, before moving to IUGR pregnancies in future.

The umbilical artery has an interesting helical geometry, measured to be approximately 0.2 coil per cm of umbilical cord at the median (Strong et al. 1994). Umbilical arterial coiling is fascinating but poorly understood (de Laet et al. 2005). Some authors attributed its formation to fetal motion, since it was observed that pathologically reduced fetal motion such as in the case of amniotic bands has reduced the number of coils, as do animals with elongated fetuses whose body

shape hinders rotation (Benirschke and Kaufmann 1995). Others have attributed the coiling to specific muscle layers within the umbilical cord, which appears to develop in the same spiral direction as the coil (Roach 1976). In about 2–5% of human fetuses, there are no coiling at all, and such a condition significantly correlated with the increased incidences of intra-uterine death, preterm delivery, intra-partum fetal heart rate decelerations and operative delivery for fetal distress (Strong et al. 1994). The quantification of fluid dynamics and WSS in the helical umbilical arteries may provide some clues to the reason for these adverse events.

In this study, we sought to characterize the *in vivo* WSS experienced by umbilical vessels, based on clinical measurements of velocities and vascular diameters, and to determine their trend with vascular diameter. Through this characterization, we also sought to investigate whether umbilical arterial coiling played a role in influencing hemodynamic conditions, specifically during the umbilical cord bending.

2 Methods

2.1 Subjects

Our study protocol was approved by National Healthcare Group (Singapore) Domain Specific Review Board, and written consents were obtained from all patient participants. This study included 28 pregnant women who underwent routine growth scan from 32nd to 33rd week of gestational age in National University Hospital, Singapore. All mothers were healthy and there was no evidence of fetal abnormalities. Ultrasonic evaluations were performed by a single sonographer, using General Electric Voluson E8 ultrasound system (GE Medical Systems Corp, Connecticut, USA) with a RAB4-8 transducer of 6MHz frequency. 3D B-mode images of the umbilical cord and pulse wave Doppler velocity measurements were acquired on the free-floating umbilical cord. The measurement was performed on one of the umbilical arteries and vein. All Doppler measurements were acquired with an insonation angle of less than 30°.

2.2 Quantitative measurements of the cross-sectional area of the umbilical vessels

To obtain the luminal cross-sectional areas of the umbilical vessels, rigorous patient-specific quantifications were performed. From the 3D B-mode ultrasound images of the umbilical cord, 3D digital reconstruction of the blood vessel geometry was performed. 3D volume file was read with 4DView® (GE Medical System, Connecticut, USA) and exported as a stack of 2D images. Contrast of the images was enhanced using a custom-written MATLAB routine to improve the ease of segmentation. The open-source soft-

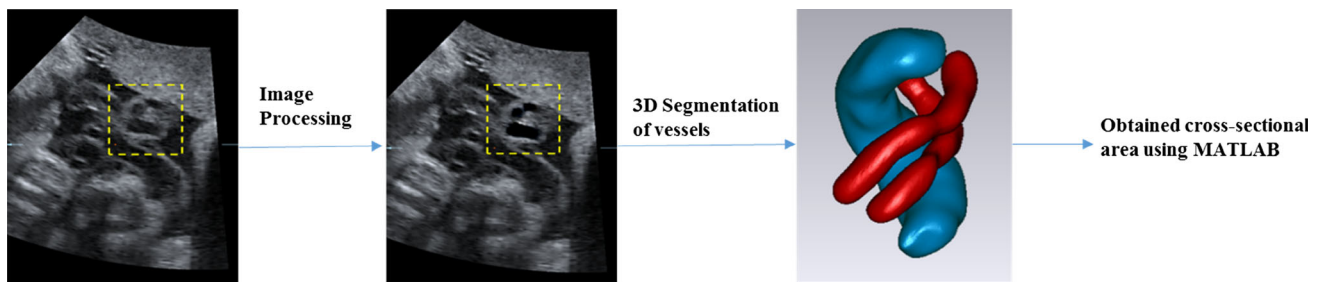


Fig. 1 Process of segmentation of umbilical vessel: Stacks of b-mode images were obtained from 3D ultrasound. Contrast of images was enhanced using written MATLAB routine in order to ease the segmen-

tation. VMTK was used to segment the umbilical arteries and umbilical vein. Finally, average cross-sectional area along the vessels was calculated using MATLAB

ware, Vascular Modeling Toolkit (VMTK) (Antiga 2006), was used to segment and reconstruct the 3D model of the umbilical cord and to smooth the reconstruction (Fig. 1). The cross-sectional area on both of the umbilical arteries and umbilical vein was sampled along the length of the blood vessels using centerline option in VMTK and averaged before being reported; cross-sectional area of both umbilical arteries was averaged and treated as a singlet artery for quantification of volumetric flow rate and WSS.

2.3 Quantification of volumetric flow rate and wall shear stress

Using the clinical scan data, fluid mechanics analysis were performed to calculate the volumetric blood flow and WSS in the umbilical arteries and vein.

2.3.1 Umbilical vein

From our pulse wave Doppler measurements and from the literature [3], blood flow velocity in umbilical vein is steady in healthy cases (Pennati et al. 1998). As the umbilical vein is relatively straight and long [approximately 50 cm (Rana et al. 1995)], the umbilical vein WSS could be approximated using Poiseuille's flow model, with a parabolic flow profile. Ultrasound measured the maximum flow velocity at the center of the parabolic profile (V_v^{US}), which was twice the mean velocity of the parabolic flow. Volumetric flow rate could thus be approximated by:

$$Q_v = \frac{V_v^{US} A_v^{US}}{2} \quad (1)$$

where A_v^{US} was the cross-sectional area of the umbilical vein. Similarly, WSS in the umbilical veins (τ_v) could be approximated by:

$$\tau_v = \frac{2\mu V_v^{US}}{R_v} \quad (2)$$

where μ was the viscosity of blood (assumed to be 0.005 Pa s (Thorburn et al. 1982)) and R_v was the radius of umbilical vein, back-computed from the measured vascular cross-sectional area, assuming perfectly circular cross section. The subscript 'v' indicated the parameters are referring to umbilical vein.

2.3.2 Umbilical artery

The umbilical arteries are generally spiral in geometry (de Laat et al. 2005) and have pulsatile flow waveforms (Adamson 1999). Previous simulation studies of the umbilical arteries (Kaplan et al. 2010) and fluid mechanics studies in helical tubes (Kao 1987; Liu and Masliyah 1993) have shown that helical pipe flow is much more complex than the simple Poiseuille flow, but thus far, a theoretical solution has not been proposed, and thus, there are no direct methods for computing flow parameters such as WSS. As such, computational modeling had to be adopted for our investigation of the umbilical artery hemodynamics.

The basic principles of spectral Doppler can be found in (Maulik 2005). Ultrasound Doppler velocity measurements were taken by sampling all velocity signals within a finite sampling volume, which was about the order of magnitude of the umbilical artery's diameter, and then providing the maximum velocity found in the sampling volume. As such, our clinical Doppler measurements provided the peak velocity of the velocity profile. Since umbilical arteries were helical in geometry, their flow profile could be far from parabolic and was not known a priori, and thus, the actual volumetric flow rate could not be directly computed. To solve this problem, an iterative scheme of CFD simulations was adopted, as explained in Fig. 2. Using our clinical Doppler ultrasound measurements (V_a^{US} , where the subscript 'a' referred to umbilical arteries), we first computed the volumetric flow rate (Q_a^{US}) by assuming a parabolic flow profile as the initial approximation. CFD simulations were first performed with this flow rate, and the maximum velocity output from the simulations (V_a^{CFD}) was compared to the Doppler ultra-

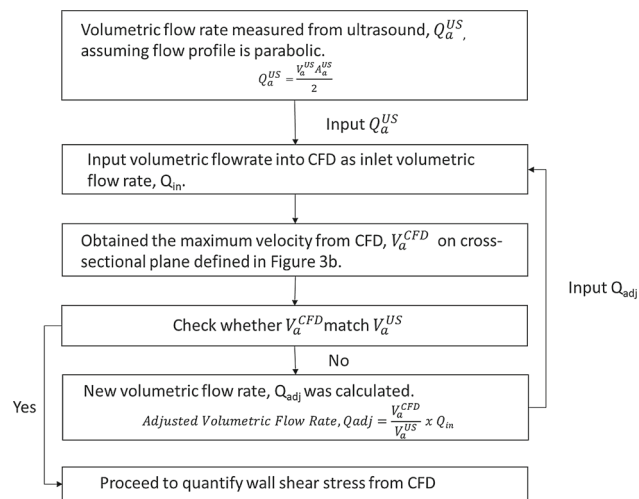


Fig. 2 Flowchart of derivation for the new volumetric flow rate, Q_{adj} , which will be input into CFD in order to match the maximum velocity obtained from CFD, V_a^{CFD} , on the cross-sectional plane with the maximum velocity measured from ultrasound, V_a^{US} . This method is applied to derive the new adjusted peak systolic, time-averaged, end diastolic and fixed volumetric flow rate during quantification of wall shear stress at three different flow conditions

sound measured maximum velocity (V_a^{US}). If a mismatch was observed, then the volumetric flow rate in the simulation was adjusted by the ratio of the simulated and measured maximum velocities, and the CFD was repeated. This iteration was repeated until a close match between the two velocities was obtained with error between two velocities being less than 1%.

A separate CFD simulation was performed for each subject scanned by adopting the umbilical artery velocity and radius, respectively. Each umbilical artery was modeled as a rigid helical pipe (Fig. 3) with a circular cross-sectional area as measured with ultrasound. Since it was difficult to measure the pitch and the helical diameter of the umbilical artery with clinical ultrasound, we adopted mean values from the literature. The umbilical coiling index (UCI), which was the number of arterial coils per cm of umbilical cord, was assumed to be 0.2 (pitch = 5 cm) (Strong et al. 1994), and the helical diameter was assumed to be 17.4 mm (Barbieri et al. 2012). The vascular cross-sectional area, UCI and helical diameter were assumed to be constant over the length of the artery. Meshing and CFD simulations were carried out using ANSYS workbench (ANSYS, Inc., Canonsburg, PA, USA). A mesh convergence analysis was performed, and the result showed that WSS computed was changed by less than 1% between a mesh of 1.2×10^6 elements to a mesh of 1.5×10^6 elements. Approximately 1.2×10^6 elements were thus used for all the cases investigated.

The Reynolds number (Re) and Womersley number (α) computed from the ultrasound vascular diameter and time-averaged mean velocity measurements were low ($Re =$

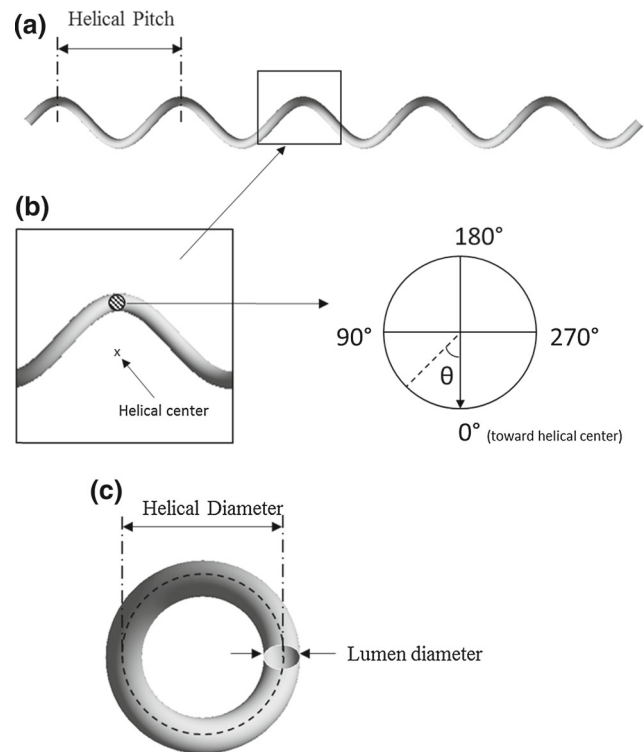


Fig. 3 a Geometry of a straight helical geometry of umbilical artery in CFD. b Cross-sectional plane of the umbilical artery lumen at mid-length. c Transverse view of helical umbilical artery

109.80 ± 29.19 ; $\alpha = 2.00 \pm 0.28$). Thus, steady-state simulations were performed. Unsteady simulation was performed on one case and compared to the steady-state simulations. The spatial distribution of WSS from the unsteady simulations, averaged over one cycle, had a satisfactory match with that from the steady simulations (performed at time-averaged Doppler velocity), as shown in Fig. 4a. Further, the flow profile from the unsteady simulations, averaged over one cycle, matched that from the steady simulations as well, as shown in Fig. 4b, c. In terms of spatially averaged WSS, results from both steady and unsteady simulations matched very well at the peak systolic and end diastolic flow conditions (<3% error). Spatially averaged WSS from unsteady simulations, averaged over one cycle, matched that from the steady simulation (performed at time-averaged Doppler velocity) well, with errors less than 5%. Based on these observations, steady flow simulations were deemed to be a suitable method in computing the in vivo WSS conditions, with reduced computational load.

Simulations were conducted at peak systolic flow rate, time-averaged flow rate and end diastolic flow rate to investigate the WSS at these different conditions. Flow was assumed to be incompressible and laminar with a density (ρ) of 1060 kg/m^3 and viscosity (μ) of 0.005 Pas (Thorburn et al. 1982). No-slip boundary condition was applied at the vas-

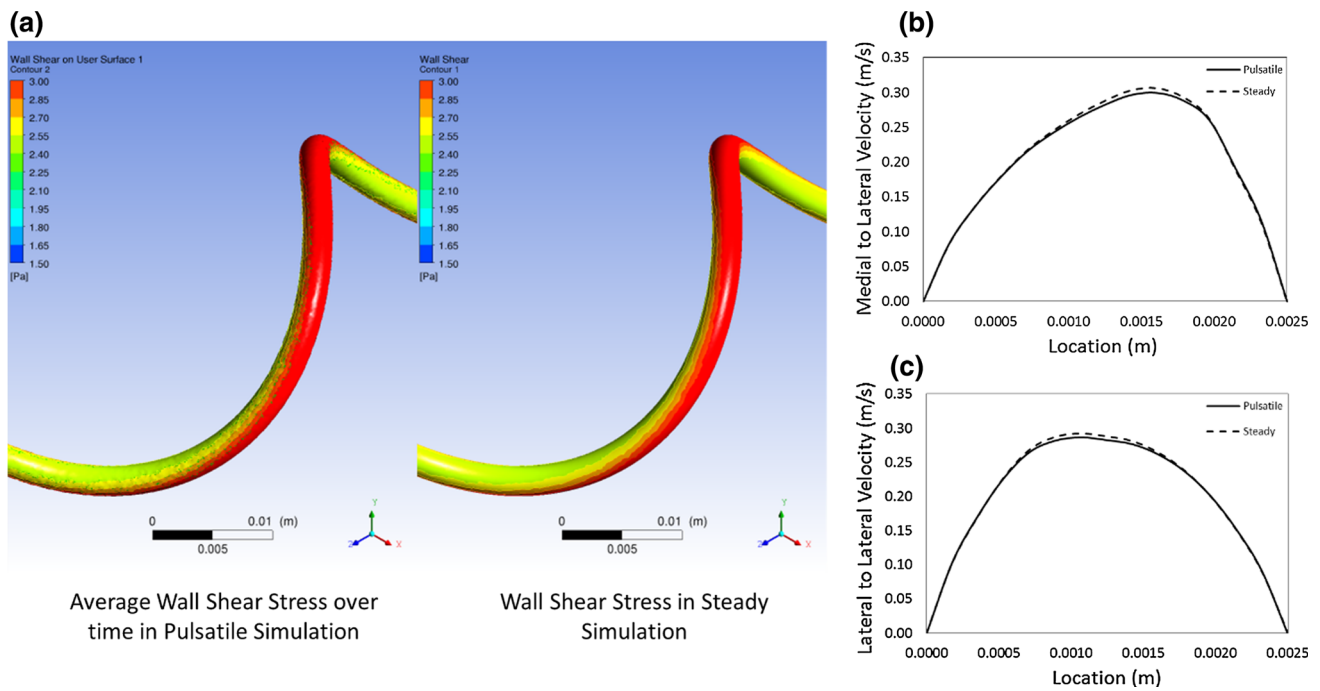


Fig. 4 Comparison between steady simulations and unsteady simulations in helical umbilical arteries. **a** WSS distribution of the unsteady simulation (averaged over one cycle) and that from the steady simulation at the time-averaged Doppler velocity. **b, c** The flow profile (plotted as absolute velocity magnitude) of the unsteady simulations (averaged over one cycle), compared to that from the steady simulation

at time-averaged Doppler velocity, plotted over the **b** medial–lateral axis (0° – 180° using convention in Fig. 3, toward/away from helical center) and **c** the lateral–lateral axis [90° – 270° , perpendicular to axis used in (b)]. A good match was observed between steady and unsteady simulations

cular walls, uniform velocity was imposed at the inlet, and uniform pressure was assumed at the outlet. The umbilical artery was modeled for 5 helical loops, and WSS results were obtained from the cross-sectional plane at the mid-length of umbilical artery (Fig. 3b). This way, 2.5 loops of the arterial vessel proximal to the cross-sectional plane and 2.5 loops distal to the cross-sectional plane acted as the flow extensions to condition the inflow and outflow. Temporal variation of WSS (obtained by comparing the simulations using peak systolic, time-averaged and end diastolic volumetric flow rates) and spatial variation of WSS (tabulated from the simulations using time-averaged volumetric flow rates) were reported.

2.3.3 Parametric studies

Regression analysis was performed to analyze the relationship between WSS and vascular diameter and that between velocity and vascular diameter. These relationships were considered significant if the *p* value was less than 0.05, suggesting that there was sufficient evidence that the regression coefficient was significantly important.

Since our CFD modeling was performed with the median values of UCI and helical diameter obtained from the literature, we also investigated the effects of varying these

parameters from the median values by performing one-way ANOVA test to compare the mean values of WSS in different geometries. The CFD analyses were performed with the following parameter changes:

1. Variations in UCI at a constant helical diameter (17.4 mm) and a constant lumen diameter (3.0 mm). Three UCI values were investigated: 0.07 (10th percentile), 0.2 (mean) and 0.3 (90th percentile) (Jessop et al. 2014).
2. Variations in helical diameter at a constant UCI (0.2) and a constant lumen diameter (3.0 mm). Three helical diameters were investigated: 13.8 mm (10th percentile), 17.4 mm (mean) and 21.1 mm (90th percentile) (Barbieri et al. 2012).

2.3.4 Effects of umbilical cord bending

The effects of umbilical cord bending on umbilical vascular hemodynamics were also conducted. Helical umbilical arterial geometry spiraling around a bent centerline of the cord was generated using the same UCI and helical diameter as above to simulate the cord bending (Fig. 5). Five different degrees of bending were investigated: the umbilical cord centerline bending with a radius of curvature 1, 2, 3, 4 and

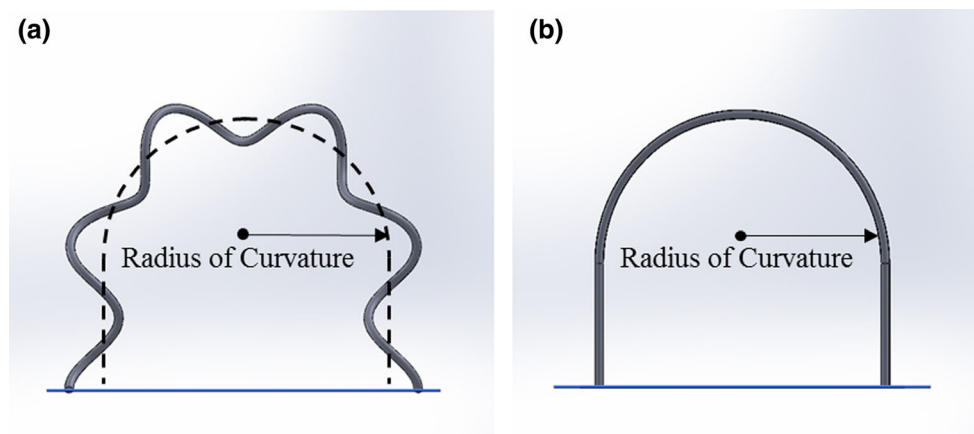


Fig. 5 **a** Helical umbilical artery after cord bending. **b** Straight umbilical artery after cord bending

5 times that of the helical diameter. At each degree of bending, four different lumen diameters (2.5, 3.0, 3.5 and 4.0 mm) were investigated, which was representative of the range of measured umbilical artery size values. Hemodynamic factors such as WSS and vascular resistance from the bent and coiled umbilical arteries (Fig. 5a) and from the bent but uncoiled umbilical arteries (Fig. 5b) were compared, while the same volumetric flow rate was imposed on both types of vessels. Pressure drop per vascular length between 40 and 60% points on the vessel centerline was computed, and resistances were computed as the ratio of pressure drop per vascular length to the volumetric flow rate.

3 Results

Mean diameter obtained from 3D quantification, time-averaged velocities measured from ultrasound, volumetric blood flow and WSS in umbilical vein and artery are summarized in Table 1. The difference in volumetric flow rate between umbilical artery and vein was found to be insignificant. Through the adoption of the iterative approach to update

boundary conditions for umbilical arteries, we incorporate realistic flow profile of the helical arteries and no longer need to assume idealized parabolic flow profile. Such an approach adjusted the values of computed arterial flow rates by 10% and led to the reduction in the difference in the computed volumetric flow rate between umbilical arteries and umbilical vein, enabling a closer fit toward the law of conservation of mass of the inflow and outflow of the placenta circulation. The difference in umbilical artery and vein volumetric flow rate was reduced from 26.84 ml/min (15.1% error) to 9.47 ml/min (5.3% error).

Clinically measured maximum blood velocity (V_a^{US} and V_v^{US} , where subscripts 'a' and 'v' refer the umbilical arteries and umbilical veins, respectively) against diameter of umbilical vessels is plotted in Fig. 6. Results showed that maximum velocity in both the umbilical artery and vein is not correlated with vascular diameter, with p values being much higher than 0.05. Two outliers were observed in the vein data. However, even after removing the outliers (umbilical vein diameters less than 0.5 cm) from Fig. 6b, the correlation was still insignificant, with p value = 0.99.

Table 1 Mean diameter, time-averaged velocity, volumetric flow rate and temporal wall shear stress at three different flow conditions and spatial wall shear stress at time-averaged volumetric flow rate in umbilical vein and umbilical artery from gestational age of 32nd to 33rd weeks

	Umbilical vein	Umbilical artery
Diameter (cm)	0.66 ± 0.10	0.31 ± 0.04
Time-averaged Velocity (cm/s), V_v^{US} or V_a^{US}	16.9 ± 3.5	32.5 ± 6.3
Volumetric flow rate (ml/min), Q_v^{US} or Q_a^{US}	177.6 ± 54.9	150.7 ± 49.2
<i>Temporal variations of WSS</i>		
Mean (Pa)	0.52 ± 0.16	2.81 ± 0.73
Peak systolic (Pa)	NA	4.90 ± 1.31
End diastolic (Pa)	NA	1.42 ± 0.42
<i>Spatial variations of WSS (at time-averaged volumetric flow rate)</i>		
Maximum WSS, at outer edge of helical coil (Pa)	NA	3.33 ± 0.49
Minimum WSS, at inner edge of helical coil (Pa)	NA	2.15 ± 0.49

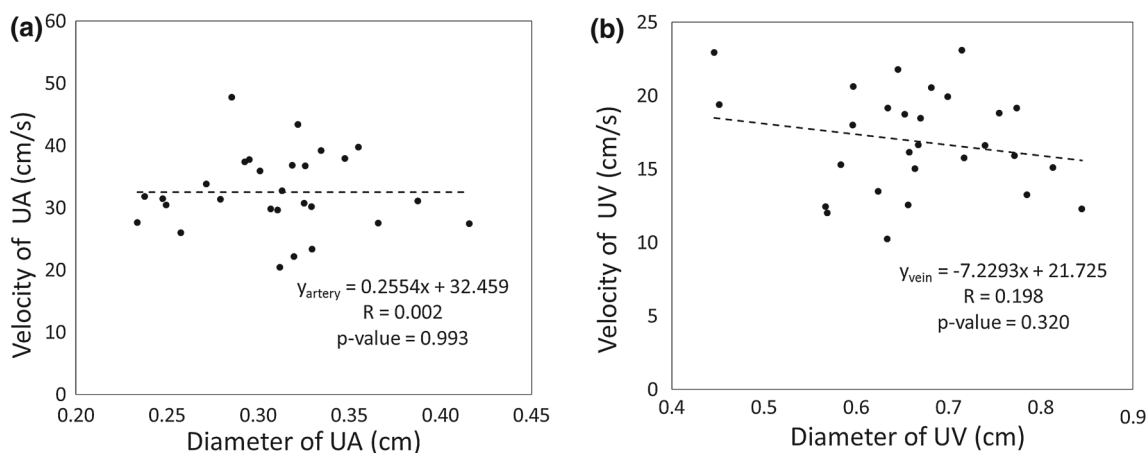


Fig. 6 Linear regression analysis demonstrating no relationship between the maximum umbilical blood velocity and diameter for cases between 32nd to 33rd gestational week for **a** umbilical artery (UA)

and **b** umbilical vein (UV). R is the correlation coefficient. p value determines the significance of coefficient of the regression line

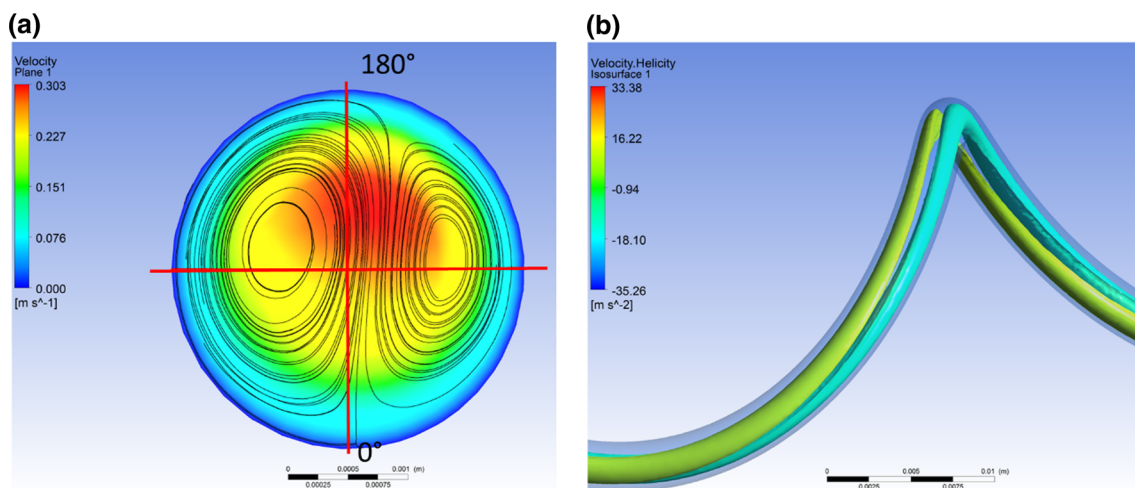


Fig. 7 **a** In-plane streamlines and absolute velocity magnitude contour on the cross-sectional plane at mid-length of the straight helical umbilical artery as defined in Fig. 3a, **b** iso-surface of helicity in the umbilical artery

Secondary flow velocity streamlines in the umbilical artery at time-averaged volumetric flow rate are shown in Fig. 7a. Two counter-rotating vortices on the cross-sectional plane at mid-length of umbilical artery, bearing resemblance to Dean Vortices (Snyder et al. 1985), were caused by centrifugal forces of curved pipe flow. These vortices were asymmetric in size, due to the helical nature of the umbilical artery geometry (Jinsuo and Benzhaio 1999), as opposed to a planar curve geometry in Dean’s flow, and the maximum velocity was skewed away from the center of the helix (as indicated by the red color velocity contour). Figure 7b, which plots helicity iso-surfaces, further demonstrates the double-helical nature of flow in the umbilical artery.

Figure 8a, b demonstrates the typical velocity profile (plotted as absolute velocity magnitude, as with the rest of Fig. 8) in the helical umbilical arteries at different artery

sizes. Figure 8a plots the flow profile along the axis that was toward/away from the center of the helix (0°–180°, the medial–lateral axis), while Fig. 8b plots the flow profile in axis perpendicular to that in Fig. 8a (90°–270°, the lateral–lateral axis). Significant deviation from the parabolic flow profile was observed, especially with the larger vessels. The profile exhibited significant skew in the direction of torsion of the helix, and the peak velocity in the profile was a significant distance from the center of the vessel. In Fig. 8b, double-peak flow profiles could be observed when the vessel was large enough. These plots also showed that the wall shear rate at the vascular walls did not change much between vessels of different sizes (slight decrease in shear rate with increasing vascular size), even though the maximum velocity of the flow profile was similar between vessels of different sizes.

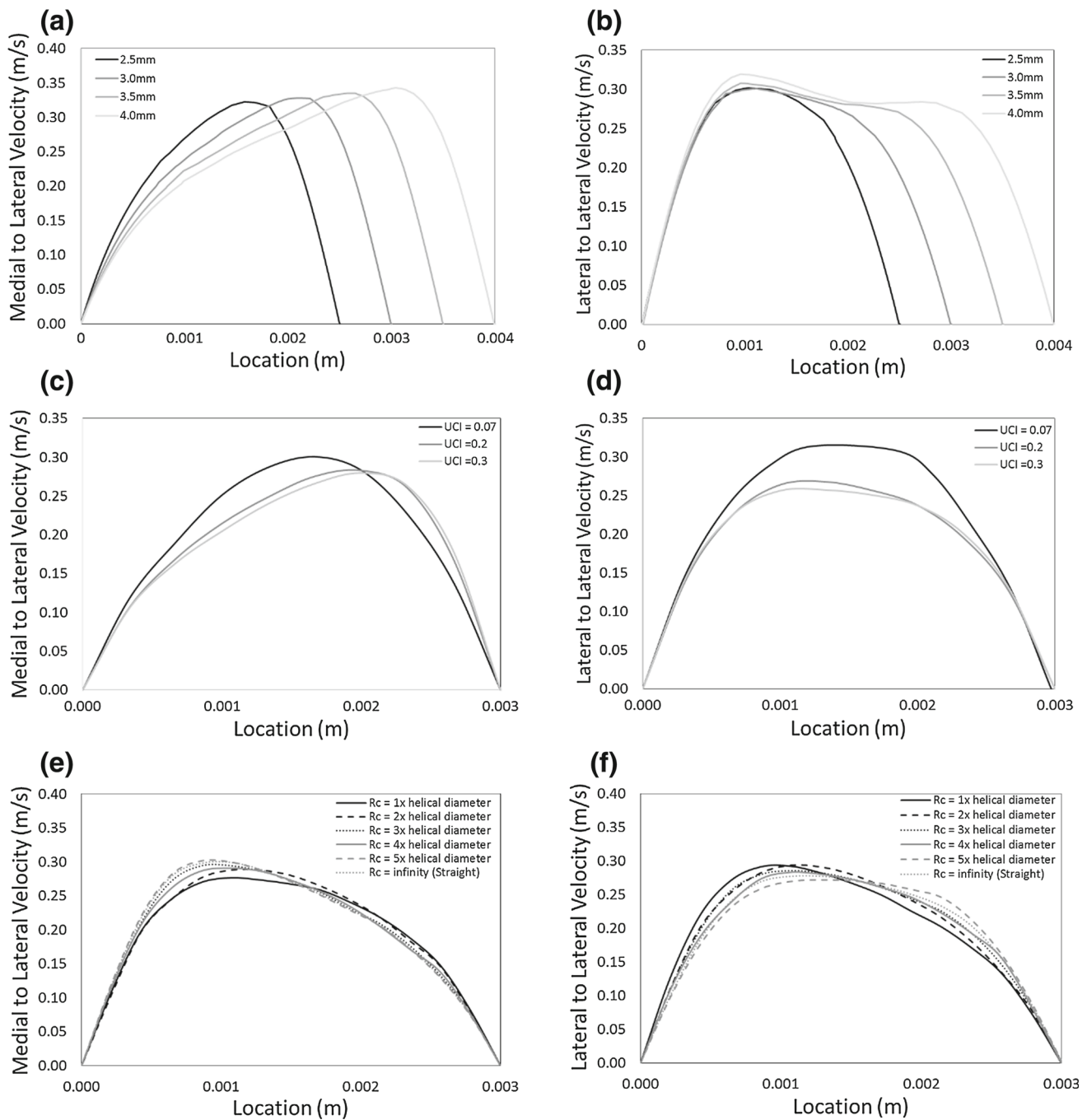


Fig. 8 Flow profiles (plotted as absolute magnitude of velocities) in the medial–lateral direction (line along 0° point to 180° point in Fig. 3b) and lateral–lateral direction (line along 90° point to 270° point in Fig. 3b) for the following conditions: **a, b** four different lumen diameters with maximum velocities according to the regression line in Fig. 6a, with

constant $UCI = 0.2$; **c, d** three different UCI with constant lumen diameters = 3.0mm and constant volumetric low rate = 66 ml/min; **e, f** various cord bending cases from no bending ($R_c = \text{infinity}$) to bending ($R_c \neq \text{infinity}$), with constant lumen diameter = 3.0 mm, constant $UCI = 0.2$ and constant volumetric flow rate = 72 ml/min

Figure 8c, d plots the flow profile in umbilical artery for different UCI, along the same two perpendicular axes used in Fig. 8a, b. Increasing UCI was observed to increase the skew in the velocity profile, and significantly altering the wall shear rate at the lateral wall, along the medial–lateral axis.

Figure 8e, f plots the flow profile for the helical umbilical cord over various degree of umbilical cord bending, also along the same axes. The flow profile did not change significantly from the case of no vascular bending ($R_c = \text{infinity}$) to cases of vascular bending ($R_c \neq \text{infinity}$) and across

various radius of curvature of the cord bending. However, slight increase in velocity profile skewness was observed when the radius of curvature of bending in the medial–lateral axis increased, but the reverse was observed in the lateral–lateral axis. The wall shear rate appeared not to change much between different degrees of bending.

WSS contour of umbilical arteries is shown in Fig. 9. As demonstrated by Fig. 9a, b, WSS at the outer edge of coil was higher than that at the inner edge of coil. Figure 9c plots the spatial distribution of WSS, averaged over all clinical cases investigated, and demonstrates the variability of WSS at specific locations. The spatial minimum, mean and maximum WSS, averaged over all clinical cases, were found 2.15, 2.81 and 3.33 Pa, respectively. These were much higher than the mean WSS (averaged over all clinical cases) for umbilical vein, which was 0.52 Pa. Figure 9d plots the spatial variation of WSS for different UCI cases. It was observed that increasing UCI increased the spatial variability of WSS. Figure 9e shows the flow profile of various umbilical artery sizes, simulated assuming Doppler velocities follow the trend line in Fig. 6a. Results showed that increasing umbilical artery size decreased WSS slightly and that the location of maximum WSS appeared to skew away from 180° in larger vessels. Figure 9f plots the flow profile of a helical umbilical artery, with the umbilical cord undergoing bending to various extent. WSS appeared to be very similar to the unbent cord state for all bending cases, except for the case of most extreme bending, where the radius of curvature was one helical diameter. In this case of highest bending, peak WSS increased, but minimum WSS remained the same as in other cases.

Figure 10 plots the WSS for all clinical cases investigated. In each case, WSS was averaged spatially before being reported. In Fig. 10a, umbilical artery WSS at peak systolic, end diastolic time points as well as at the time-averaged flow rate was shown. WSS, when plotted against the diameter of the umbilical arteries, showed a slight decreasing trend. However, this relationship was not statistically significant. The slight decreasing trend was confirmed by Fig. 10c, where umbilical arteries of idealized sizes (0.25, 0.30, 0.35 and 0.4 cm) were analyzed assuming the Doppler velocities described by the regression line in Fig. 6a. These simulations were not based on individual clinical measurement cases, but were performed to understand the sensitivity of arterial WSS by changing the diameter without the variability of the clinical data to shroud the trend. The result showed that WSS can be described by this empirical equation:

$$\text{WSS} = -2.984 \times \text{diameter} + 3.6703 \quad (3)$$

Figure 10b plots the WSS in the umbilical vein. A significant decreasing trend of WSS with vascular diameter (p value <0.0001) was observed, which contrasted from the observations in umbilical arteries. Considering that the

two outliers (umbilical vein diameters less than 0.5 cm) in Fig. 10b might affect the results, we re-performed the regression analysis after removing the two outliers, but found that the p value was still significant, at 0.03.

The parametric simulations performed demonstrated the effect of UCI and helical diameter on the mean WSS in the vessels. Results showed that mean WSS was affected by UCI, whereas WSS increased steadily with increasing UCI. Helical diameter, however, did not affect mean WSS (Fig. 11a).

As for umbilical cord bending, results are shown in Fig. 11b. WSS and flow resistance in the helical umbilical artery did not change much from the case with no bending to cases with bending, up to when the radius of curvature was $2\times$ helical diameters. When the umbilical cord was further bent to a radius of curvature of $1\times$ helical diameter, WSS and flow resistance increased. In contrast, in uncoiled tubes with no helical features but with matching volumetric flow rates as coiled tubes, WSS and flow resistance increased linearly with the reciprocal of radius of curvature of cord bending. These uncoiled tube cases were representative of the conditions experienced by umbilical veins, although the vein flow rate and sizes were different.

4 Discussions

In this study, we investigated the flow patterns and WSS levels in umbilical artery environments obtained from individual patients ultrasound data.

From our results, it was clear that the flow profile in the umbilical arteries could be very different from that of a Poiseuille flow parabolic profile, due to its helical geometry, especially when the arterial diameter was large. The flow profile also changed rather drastically from that in small vessels to that in large vessels. Consequently, both the maximum velocity of the flow profile and WSS experienced by the vessel could have no correlation with vascular diameter (as shown in Figs. 6a, 10a), in contrast to the theory of Poiseuille flow. In Poiseuille flow, having a constant maximum velocity of flow profile across different vascular diameters must result in significant changes to WSS across different vascular diameters.

By adopting realistic, non-Poiseuille flow profile in our analysis of umbilical arteries, we found that there was a better match between umbilical artery volumetric flow rate and umbilical vein volumetric flow rate (errors decreased from 15.1 to 5.3 %, which became insignificant). A better adherence to the principles of conservation of mass of the inflow and outflow of the placenta circulation was observed. In fact, earlier studies had encountered a similar mismatch problem: Lees et al. (1999) measured the volumetric flow rate of umbilical veins to be 400 ml/min and that in the umbilical arteries to be 450 ml/min, an 11 % mismatch. We thus believe that our

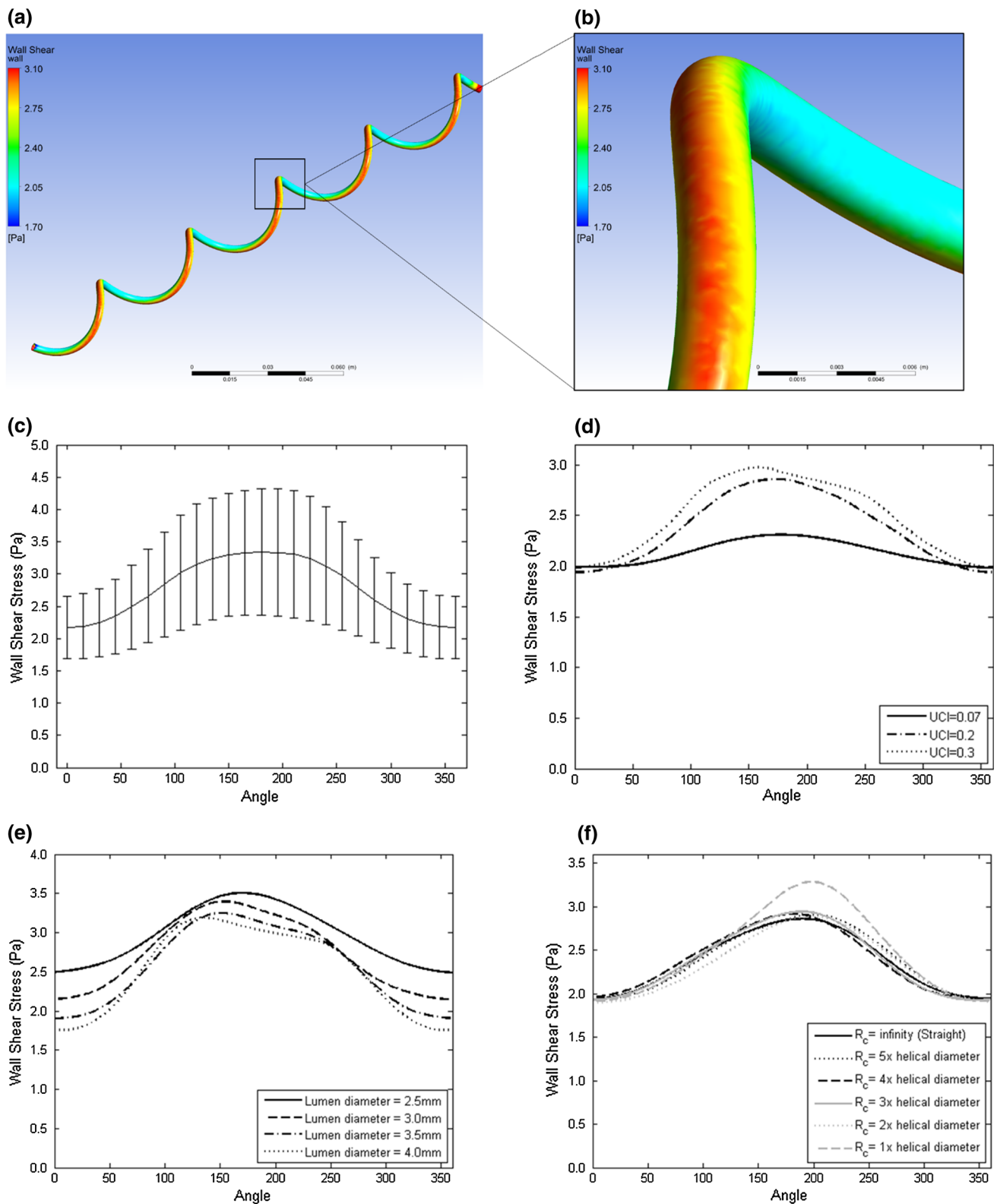


Fig. 9 **a** Wall shear stress contour on the umbilical artery. **b** Zoom in wall shear stress on the mid-length of umbilical artery. **c** Wall shear stress distribution along the perimeter of cross-sectional plane at mid-length of umbilical artery, as defined in Fig. 3b, as the mean and standard deviation of the 28 clinical cases. Wall shear stress distribution for dif-

ferent **d** UCI (constant lumen diameter and helical diameter), **e** lumen diameters (constant UCI and helical diameter) and **f** various cord bending from no bending ($R_c = \text{infinity}$) to bending ($R_c \neq \text{infinity}$) as illustrated in Fig. 5a (constant UCI and lumen diameter)

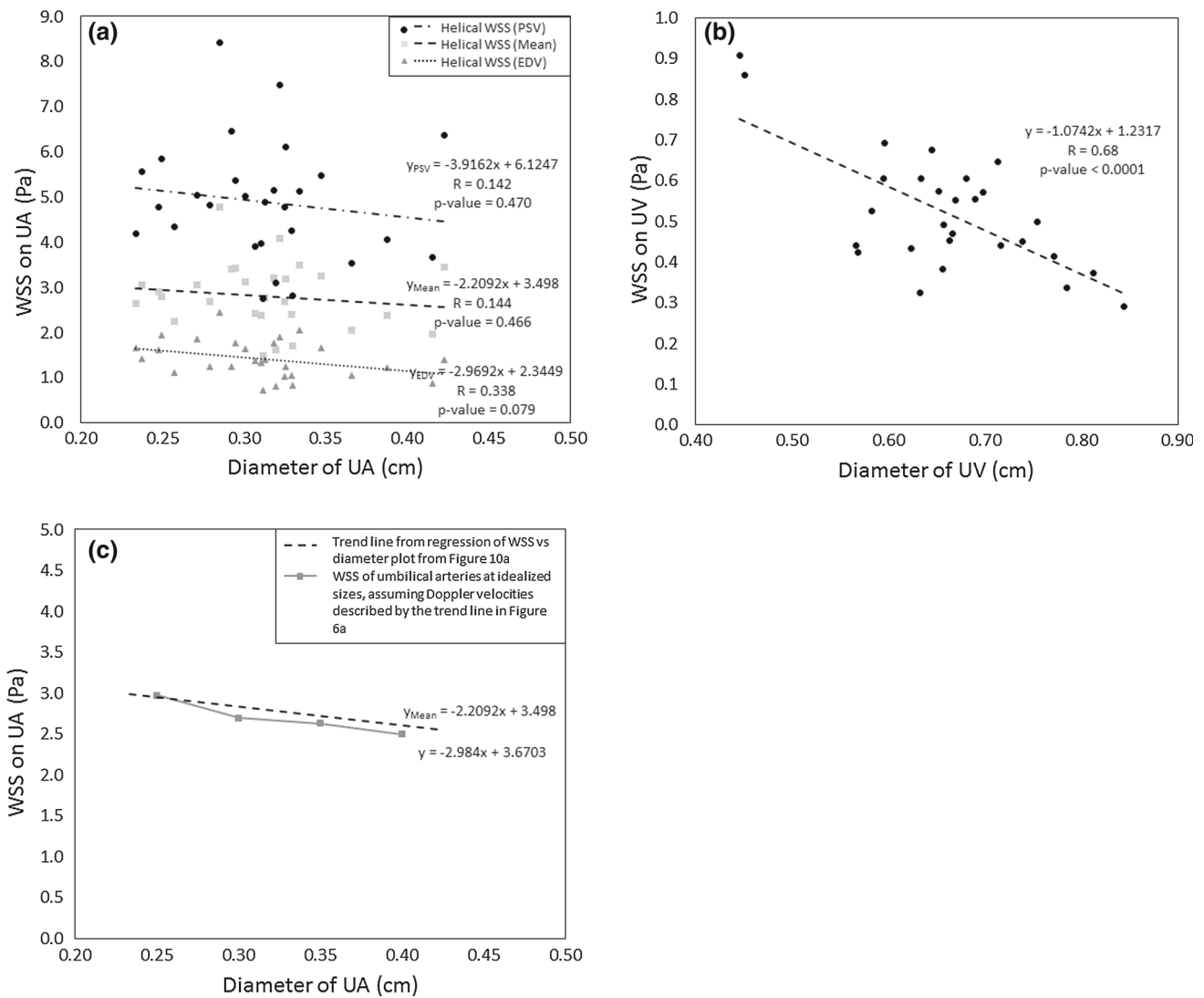


Fig. 10 Linear regression analysis between mean wall shear stress and diameter for cases from 32nd to 33rd gestational weeks for **a** umbilical artery (UA) and **b** umbilical vein (UV). **c** Comparison of WSS trend line from the clinical data (*dashed black line*) with the idealized simu-

lations at four different arterial diameters (*solid gray line*) with Doppler velocity obtained from the regression line in Fig. 6a. *R* is a correlation coefficient. *p* value determines the significance of coefficient of the regression line

iterative matching CFD technique allowed a more accurate computation of volumetric flow rate by considering the helical geometry of the umbilical artery and adopting realistic flow profiles.

One of our major observations in the study was the WSS differences between the umbilical arteries and veins. In arteries, both velocity and WSS did not correlate with vascular diameter. However, in the veins, while velocity did not correlate with vascular diameter, WSS had a significant decreasing trend with increasing vascular size. For example, from the smallest umbilical artery to the largest, WSS decreased about 14%, but from the smallest umbilical vein to the largest, WSS decreased about 57%. This difference was the consequence of the geometric difference between the umbilical

artery and vein, where one was helical and the other was straight.

We speculate that this insignificant relationship of WSS with diameters in the arteries might indicate the presence of WSS homeostatic regulation where the ECs responded to WSS by sending signals for the growth or regression of the vessel. High WSS would thus be reduced through vascular growth, and low WSS increased through vascular regression or reduced growth, such that WSS would be self-modulated toward a baseline level. This mechanism was also proposed by other authors, who found a similar lack of correlation between WSS and vascular size in human fetal descending aorta (Struijk et al. 2005), fetal mice artery (Yap et al. 2014) and monkey artery (Zarins et al. 1987). Our data corroborated

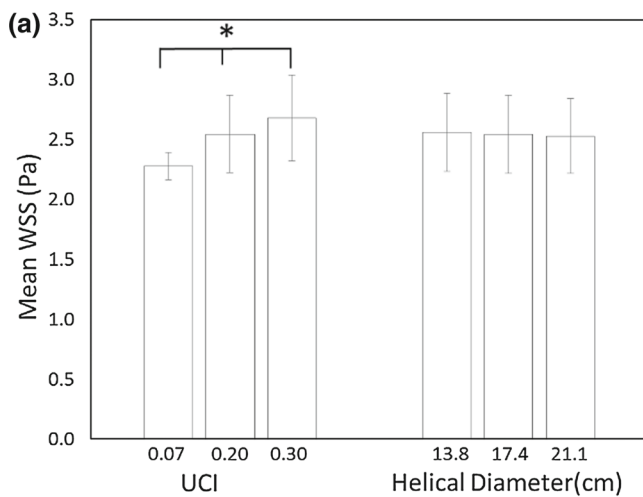
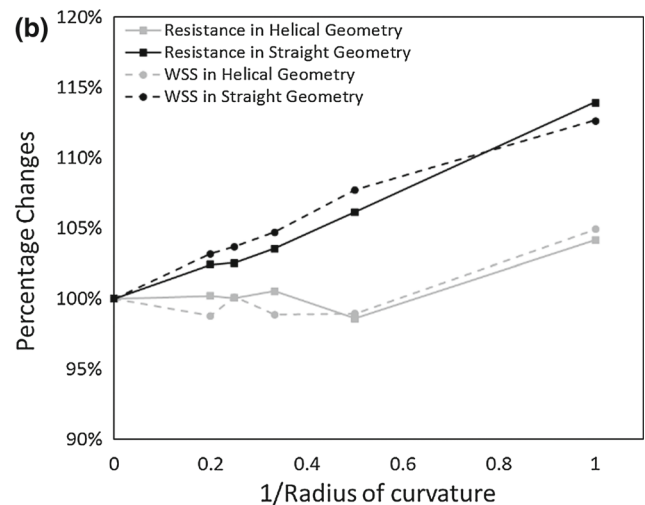


Fig. 11 a Mean wall shear stress in different umbilical coiling index (UCI) and helical diameter. The *error bar* represents the variation of wall shear stress along the perimeter of cross-sectional plane at mid-length of umbilical artery, as defined in Fig. 3b. One-way ANOVA test was performed, and **p* value <0.0001. **b** Percentage changes of resistance and mean wall shear stress in bent helical umbilical artery



(Fig. 4a) and bent straight umbilical artery (Fig. 4b) with respect to the reference value which is set to be helical umbilical artery without bending (Fig. 3a). $1/R_c = 0.0$ represents unbent umbilical artery, while $1/R_c = 1.0$ represents extreme bent umbilical artery with $R_c = 1x$ of umbilical artery's helical diameter

with this theory, but did not prove it, and further investigations are much warranted.

In the umbilical vein, however, the same lack of correlation between WSS and vascular size was not present. We speculate that because the umbilical vein utilized different cues for vascular remodeling than arteries. Previous authors has provided evidence that the gene expression is controlled differently in venous environment and arterial environment as shown by several authors (Adams et al. 1999; Kim et al. 2008; Korten et al. 2013). For example, Wang et al. (1998) showed that ephrin-B2, which is involved in mediating vascular development (Wang et al. 2010), marks the onset of angiogenesis in arterial but not in venous ECs. Furthermore, the growth of the umbilical vein might be responding to the growth needs of a fetus instead of responding to the WSS exerted on the vein's wall because umbilical vein is the main vessel that transports the oxygen and nutrients to the fetus. These findings may provide an explanation for the differences between the umbilical artery and vein WSS and velocities in our study.

Another interesting observation from our study was that the spiral geometry of the umbilical artery provided the vessel with greater constancy of WSS and vascular resistance in the event of cord bending. In the womb, umbilical cords, being long and flexible structures, tend to bend and turn around. Our results showed that bending of helical umbilical artery did not affect the WSS or flow resistance much, except when the extent of bending was very high. In contrast, the WSS and flow resistance in non-helical (straight) vessel increased steadily, even with low extent of bending.

This suggested that the helical geometry provided a more stable hemodynamic condition to the umbilical arteries, but the same stabilization protection was not present in the veins. We hypothesize that this helical feature could be an adaptation to enable the umbilical artery to sense hemodynamic flow rates without being interfered by cord bending. This notion corroborates with the hypothesis that the umbilical artery actively senses WSS for remodeling cues. We further hypothesize that the observed correlation between uncoiled umbilical arteries and increased incidences of pregnancy complications (Strong et al. 1994) could be due to the uncoiled artery being unable to maintain constancy in the umbilical-placental circulation environment.

In our study, we adopted a robust method in quantifying the volumetric flow rate in umbilical arteries and vein by measuring the cross-sectional area from 3D acquisitions (for both umbilical arteries and vein). 3D quantification of cross-sectional area is generally better than the conventional 2D approach because 2D acquisition of cross-sectional area can result in misalignment of the plane of imaging with the vessel diameter, resulting in the measurement of a chord of the circular cross section instead of the diameter. When we had used 2D vascular size quantification, the discrepancy between umbilical arterial flow rate and umbilical venous flow rate was 36%, but the discrepancy reduced to 5.3% with 3D quantifications. This improved our ability to abide by the principle of mass conservation for flow going into and out of the placenta.

As expected from the helical geometry, CFD results showed the presence of a pair of asymmetric Dean vortices

(Dean and Hurst 1959) (Fig. 7a, b), which were the result of centrifugal force in flow navigating through curved channels. Flow in helical tubes has been studied previously and is known to manifest either a partial or complete dominance of one of the two vortices, depending on the geometry and flow conditions (Liu and Masliyah 1993). In the case of 32–33 weeks umbilical arteries, only a partial dominance of one of the two vortices was observed. Consequent to this asymmetry, a spatial variation in WSS was observed: WSS was higher on the outer edge of the coil than on the inner edge of the coil. The magnitude difference between the maximum WSS and minimum WSS was substantial, being more than 50% of the minimum value. This complex WSS environment should be noteworthy for investigators using umbilical arterial ECs for shear stress mechanobiology experiments, as these differential native conditions may have preconditioned the cells from the outer edge of coil to have different biological responses from those from the inner edge of coil, although this notion is currently an untested hypothesis.

Our WSS magnitude results compared well with those from other investigations. Struijk et al. (2005) showed the WSS in human fetus descending aorta to be 2.2 Pa across the gestational age of 19–38 weeks. In our current study, the magnitude of temporally and spatially averaged WSS in 32–33 weeks human umbilical arteries was 2.8 Pa, close to Struijk et al.'s measurements. In the umbilical vein, mean WSS was approximately 0.52 Pa. There is a lack of studies on the WSS in fetus vein, but our venous WSS value compared well with WSS measured in adult veins (0.6 Pa) (Misra et al. 2009, 2006).

Umbilical vein ECs are popularly used in in vitro mechanobiology experiments, for example, to investigate the atheroprotective effect of laminar WSS in ECs. In these experiments, however, investigators often assumed the baseline WSS of these ECs to be around 1.6–2.5 Pa (or 16–25 dynes/cm²) (McCormick et al. 2001; Yoshizumi et al. 2003; Zhang et al. 2013), as is the physiological value in adult arteries. The results of our study showed that the umbilical vein ECs' native WSS (0.5 Pa or 5 dynes/cm²) is much lower than the values used in in vitro experiments. On the other hand, the umbilical arterial EC's WSS environment (2.8 Pa) may have a better match with conditions in these in vitro experiments simulating arterial environments and may be better cell sources. This is especially so when recent studies are gathering evidence that the gene expression is controlled differently in arterial and venous environment (Handwerker et al. 1990; Takamura et al. 1990).

In our study, we investigated the effects of UCI and helical diameter on WSS of umbilical arteries because these two parameters were not readily available from our clinical data. Our results showed that WSS was significantly different if different UCI values were used for analysis. For instance, utilizing 10th percentile (UCI = 0.07) and 90th

percentile (UCI = 0.3) of UCI would cause 7% deviation in WSS, when compared to using the mean UCI (UCI = 0.2). However, many studies have shown that the UCI in normal pregnancy is 0.2 (Jessop et al. 2014; Strong et al. 1994; van Diik et al. 2002), and the UCI of 0.07 and 0.3 is only present in abnormal pregnancy (de Laat et al. 2005). As our study involved only normal pregnancy, UCI = 0.2 was thus the most appropriate choice. As for helical diameter, it was found to have negligible influence on WSS within the physiological ranges of helical diameter and was thus unimportant in our WSS quantification.

Our current study was built on the foundation of a previous study by Kaplan et al. (2010), which studied the flow dynamics in the umbilical arteries with various helical coiling characteristics. Some of our observations described above, for example, the observation that some umbilical arteries featured a double maximum flow profile along one axis, and a skewed single maximum flow profile along the perpendicular axis, agreed with that observed by Kaplan et al. Our observation which showed that the UCI significantly affected the flow dynamics of the umbilical artery also agreed with Kaplan et al.'s results. In the current study, we have extended Kaplan et al.'s work by including clinically measured velocity conditions, effects of varying artery sizes and the effect of umbilical cord bending.

In conclusion, we performed an investigation on the WSS environments of the human fetal umbilical vessels at 32–33 weeks. Our results showed key differences in the WSS environment of the umbilical arteries and veins. WSS was one order of magnitude higher in umbilical arteries than veins, and while there was no correlation between WSS and vascular diameter in the umbilical artery, a strong correlation was found in the umbilical vein. Finally, we discovered that the helical geometry of the umbilical artery appeared to guard against hemodynamic changes in the event of umbilical cord bending, potentially uncovering the function of the helical shape of the vessel.

5 Limitations

The first limitation in our study was that the CFD simulation was performed based on the assumptions that umbilical artery was rigid, which was not the case in reality. However, the systolic distention of the umbilical artery was not expected to be more than 3% (Urban et al. 2009), since umbilical pressures have a pulse pressure of approximately 25 mmHg (Struijk et al. 2008), and the compliance of the umbilical artery per unit length was found to be approximately 2.54×10^{-5} ml/mmHg.

Secondly, because we were unable to quantify the UCI from clinical scans, we adopted the clinical mean UCI value as reported in the literature. UCI, however, was found to

significantly affect the WSS. The lack of patient-specific UCI in our study was thus a limitation to our approach.

Acknowledgements This study was supported by the NMRC-CRBNIG Grant by the Ministry of Health (Grant Number: NMRC/BNIG/2020/2014, PI: Yap Choon Hwai). We thank Nyien Chan Ko Ko for his assistance in the data processing.

Compliance with ethical standards

Conflict of interest All authors have no conflict of interest to declare.

References

- Adams RH et al (1999) Roles of ephrinB ligands and EphB receptors in cardiovascular development: demarcation of arterial/venous domains, vascular morphogenesis, and sprouting angiogenesis. *Genes Dev* 13:295–306
- Adamson SL (1999) Arterial pressure, vascular input impedance, and resistance as determinants of pulsatile blood flow in the umbilical artery. *Eur J Obstet Gynecol* 84:119–125. doi:10.1016/S0301-2115(98)00320-0
- Antiga LaDS (2006) VMTK-vascular modeling toolkit. <http://www.vmtk.org>
- Barbieri C, Cecatti JG, Surita FG, Marussi EF, Costa JV (2012) Sonographic measurement of the umbilical cord area and the diameters of its vessels during pregnancy. *J Obstet Gynaecol* 32:230–236. doi:10.3109/01443615.2011.647129
- Benirschke K, Kaufmann P (1995) Pathology of the human placenta. Springer, New York
- Boito S, Struijk PC, Ursem NTC, Stijnen T, Wladimiroff JW (2002) Umbilical venous volume flow in the normally developing and growth-restricted human fetus. *Ultrasound Obstet Gynecol* 19:344–349. doi:10.1046/j.1469-0705.2002.00671.x
- Cheng C et al (2005) Shear stress affects the intracellular distribution of eNOS: direct demonstration by a novel in vivo technique. doi:10.1182/blood-2005-06-2326
- de Laat M, Franx A, van Alderen E, Nikkels P, Visser G (2005) The umbilical coiling index, a review of the literature. *J Matern Fetal Neonatal Med* 17:93–100
- Dean WR, Hurst JM (1959) Note on the motion of fluid in a curved pipe. *Mathematika* 6:77–85. doi:10.1112/S0025579300001947
- dela Paz NG, Walshe TE, Leach LL, Saint-Geniez M, D'Amore PA (2012) Role of shear-stress-induced VEGF expression in endothelial cell survival. *J Cell Sci* 125:831–843
- Gardosi J, Clausson B, Francis A (2009) The value of customised centiles in assessing perinatal mortality risk associated with parity and maternal size. *BJOG* 116:1356–1363. doi:10.1111/j.1471-0528.2009.02245.x
- Handwerker SM, Halevy S, Altura BM (1990) Effects of vasoactive agents on isolated human umbilical veins in preeclamptic women. *Magn Trace Elements* 9:70–78
- Hsieh HJ, Li NQ, Frangos JA (1991) Shear stress increases endothelial platelet-derived growth factor mRNA levels. *Am J Physiol* 260(2 Pt 2):H642–H646
- Jessop FA, Lees CC, Pathak S, Hook CE, Sebire NJ (2014) Umbilical cord coiling: clinical outcomes in an unselected population and systematic review. *Virchows Arch* 464:105–112. doi:10.1007/s00428-013-1513-2
- Jinsuo Z, Benzhuo Z (1999) Fluid flow in a helical pipe. *Acta Mech Sin* 15:299–312. doi:10.1007/BF02487928
- Kao HC (1987) Torsion effect on fully developed flow in a helical pipe. *J Fluid Mech* 184:335–356
- Kaplan AD, Jaffa AJ, Timor IE, Elad D (2010) Hemodynamic analysis of arterial blood flow in the coiled umbilical cord. *Reprod Sci* 17:258–268
- Kim JS et al (2008) Gene expression profiling demonstrates a novel role for foetal fibrocytes and the umbilical vessels in human fetoplacental development. *J Cell Mol Med* 12:1317–1330. doi:10.1111/j.1582-4934.2008.00284.x
- Korten S et al (2013) Impact of Hey2 and COUP-TFII on genes involved in arteriovenous differentiation in primary human arterial and venous endothelial cells. *Basic Res Cardiol* 108:362. doi:10.1007/s00395-013-0362-0
- Lawn JE, Cousens S, Zupan J, Steering Lancet Neonatal Survival T (2005) 4 Million neonatal deaths: when? where? why? *Lancet* 365:891–900. doi:10.1016/S0140-6736(05)71048-5
- Lees C, Albaiges G, Deane C, Parra M, Nicolaides KH (1999) Assessment of umbilical arterial and venous flow using color Doppler. *Ultrasound Obstet Gynecol* 14:250–255. doi:10.1046/j.1469-0705.1999.14040250.x
- Liu S, Masliyah JH (1993) Axially invariant laminar flow in helical pipes with a finite pitch. *J Fluid Mech* 251:315–353
- Malek AM, Alper SL, Izumo S (1999) Hemodynamic shear stress and its role in atherosclerosis. *JAMA* 282:2035–2042
- Maulik D (2005) Spectral Doppler: basic principles and instrumentation. In: Maulik D (ed) Doppler ultrasound in obstetrics and gynecology. Springer, New York, pp 19–34
- McCormick SM, Eskin SG, McIntire LV, Teng CL, Lu C-M, Russell CG, Chittur KK (2001) DNA microarray reveals changes in gene expression of shear stressed human umbilical vein endothelial cells. *Proc Nat Acad Sci* 98:8955–8960
- Misra S, Misra WDA et al (2006) Assessment of wall shear stress changes in arteries and veins of arteriovenous polytetrafluoroethylene grafts using magnetic resonance imaging. *Cardiovasc Interv Radiol* 29:624–629. doi:10.1007/s00270-005-0168-z
- Misra S, Fu AA, Misra KD, Glockner JF, Mukhopadhyay D (2009) Wall shear stress measurement using phase contrast magnetic resonance imaging with phase contrast magnetic resonance angiography in arteriovenous polytetrafluoroethylene grafts. *Angiology* 60:441–447. doi:10.1177/0003319709335908
- Nagel T, Resnick N, Dewey CF, Gimbrone MA (1999) Vascular endothelial cells respond to spatial gradients in fluid shear stress by enhanced activation of transcription factors. *Arterioscler Thromb Vasc Biol* 19:1825–1834. doi:10.1161/01.atv.19.8.1825
- Nakatsu MN et al (2003) VEGF(121) and VEGF(165) regulate blood vessel diameter through vascular endothelial growth factor receptor 2 in an in vitro angiogenesis model. *Lab Invest* 83:1873–1885
- Pennati G, Bellotti M, Ferrazzi E, Bozzo M, Pardi G, Fumero R (1998) Blood flow through the ductus venosus in human fetus: calculation using Doppler velocimetry and computational findings. *Ultrasound Med Biol* 24:477–487. doi:10.1016/S0301-5629(98)00011-8
- Raio L, Ghezzi F, Di Naro E, Duwe DG, Cromi A, Schneider H (2003) Umbilical cord morphologic characteristics and umbilical artery Doppler parameters in intrauterine growth-restricted fetuses. *J Ultrasound Med* 22:1341–1347
- Rana J, Ebert GA, Kappy KA (1995) Adverse perinatal outcome in patients with an abnormal umbilical coiling index. *Obstet Gynecol* 85:573–577
- Roach M (1976) The umbilical vessels Perinatal medicine: the basic science underlying clinical practice. Williams and Wilkins, Baltimore
- Smiesko V, Kozik J, Dolezal S (1985) Role of endothelium in the control of arterial diameter by blood flow. *Blood Vessels* 22:247

- Snyder B, Hammersley JR, Olson DE (1985) The axial skew of flow in curved pipes. *J Fluid Mech* 161:281–294. doi:[10.1017/S0022112085002932](https://doi.org/10.1017/S0022112085002932)
- Strong TH Jr, Jarles DL, Vega JS, Feldman DB (1994) The umbilical coiling index. *Am J Obstet Gynecol* 170:29–32. doi:[10.1016/S0002-9378\(94\)70378-7](https://doi.org/10.1016/S0002-9378(94)70378-7)
- Struijk PC, Stewart PA, Fernando KL, Mathews VJ, Loupas T, Steegers EAP, Wladimiroff JW (2005) Wall shear stress and related hemodynamic parameters in the fetal descending aorta derived from color Doppler velocity profiles. *Ultrasound Med Biol* 31:1441–1450. doi:[10.1016/j.ultrasmedbio.2005.07.006](https://doi.org/10.1016/j.ultrasmedbio.2005.07.006)
- Struijk PC, Mathews VJ, Loupas T, Stewart PA, Clark EB, Steegers EA, Wladimiroff JW (2008) Blood pressure estimation in the human fetal descending aorta. *Ultrasound Obstet Gynecol* 32:673–681. doi:[10.1002/uog.6137](https://doi.org/10.1002/uog.6137)
- Takamura H, Kasai H, Arita H, Kito M (1990) Phospholipid molecular species in human umbilical artery and vein endothelial cells. *J Lipid Res* 31:709–717
- Thornburn J, Drummond MM, Whitgham KA, Lowe GDO, Forbes CD, Prentice CRM, Whitfield CR (1982) Blood viscosity and haemostatic factors in late pregnancy, pre-eclampsia and fetal growth retardation. *BJOG* 89:117–122. doi:[10.1111/j.1471-0528.1982.tb04676.x](https://doi.org/10.1111/j.1471-0528.1982.tb04676.x)
- Traub O, Berk BC (1998) Laminar shear stress: mechanisms by which endothelial cells transduce an atheroprotective force. *Arterioscler Thromb Vasc Biol* 18:677–685. doi:[10.1161/01.atv.18.5.677](https://doi.org/10.1161/01.atv.18.5.677)
- Urban G et al (2009) 289: Predicting perinatal outcome through changes in umbilical artery wall distension rate and turbulence index in severely growth-restricted fetuses. *Am J Obstet Gynecol* 201:S117–S117. doi:[10.1016/j.ajog.2009.10.304](https://doi.org/10.1016/j.ajog.2009.10.304)
- van Diik CC, Franx A, de Laat MW, Bruinse HW, Visser GH, Nikkels PG (2002) The umbilical coiling index in normal pregnancy. *J Matern fetal Neonatal Med* 11:280–283. doi:[10.1080/jmf.11.4.280.283](https://doi.org/10.1080/jmf.11.4.280.283)
- Vinkesteijn ASM, Struijk PC, Ursem NTC, Hop WCJ, Wladimiroff JW (2004) Fetal heart rate and umbilical artery flow velocity variability in intrauterine growth restriction: a matched controlled study. *Ultrasound Obstet Gynecol* 23:461–465. doi:[10.1002/uog.1032](https://doi.org/10.1002/uog.1032)
- Wang HU, Chen Z-F, Anderson DJ (1998) Molecular distinction and angiogenic interaction between embryonic arteries and veins revealed by ephrin-B2 and its receptor Eph-B4. *Cell* 93:741–753. doi:[10.1016/S0092-8674\(00\)81436-1](https://doi.org/10.1016/S0092-8674(00)81436-1)
- Wang Y et al (2010) Ephrin-B2 controls VEGF-induced angiogenesis and lymphangiogenesis. *Nature* 465:483–486. http://www.nature.com/nature/journal/v465/n7297/supinfo/nature09002_S1.html
- Yap CH, Liu X, Pekkan K (2014) Characterization of the vessel geometry, flow mechanics and wall shear stress in the great arteries of wildtype prenatal mouse. *PLoS One* 9(1):e86878
- Yoshizumi M, Kurihara H, Sugiyama T, Takaku F, Yanagisawa M, Masaki T, Yazaki Y (1989) Hemodynamic shear stress stimulates endothelin production by cultured endothelial cells. *Biochem Biophys Res Commun* 161:859–864. doi:[10.1016/0006-291X\(89\)92679-X](https://doi.org/10.1016/0006-291X(89)92679-X)
- Yoshizumi M, Abe J, Tsuchiya K, Berk BC, Tamaki T (2003) Stress and vascular responses: atheroprotective effect of laminar fluid shear stress in endothelial cells: possible role of mitogen-activated protein kinases. *J Pharmacol Sci* 91:172–176
- Zarins CK, Zatina MA, Giddens DP, Ku DN, Glagov S (1987) Shear stress regulation of artery lumen diameter in experimental atherogenesis. *J Vasc Surg* 5:413–420. doi:[10.1016/0741-5214\(87\)90048-6](https://doi.org/10.1016/0741-5214(87)90048-6)
- Zhang F, Zhang L, Sun L-l, Meng X-l, Zhao Y, Jin X (2013) Effects of fluid shear stress on expression of smac/DIABLO in human umbilical vein endothelial cells. *Curr Ther Res Clin Exp* 74:36–40. doi:[10.1016/j.curtheres.2012.11.002](https://doi.org/10.1016/j.curtheres.2012.11.002)